JCIM JOURNAL OF CHEMICAL INFORMATION AND MODELING

pubs.acs.org/jcim Article

Physical Chemistry of Chloroquine Permeation through the Cell Membrane with Atomistic Detail

Mirko Paulikat, GiovanniMaria Piccini, Emiliano Ippoliti, Giulia Rossetti, Fabio Arnesano, and Paolo Carloni*

Cite This: J. Chem. Inf. Model. 2023, 63, 7124−7132 Read Online

ABSTRACT: We provide a molecular-level description of the thermodynamics and mechanistic aspects of drug permeation through the cell membrane. As a case study, we considered the antimalaria FDA approved drug chloroquine. Molecular dynamics simulations of the molecule (in its neutral and protonated form) were performed in the presence of different lipid bilayers, with the aim of uncovering key aspects of the permeation process, a fundamental step for the drug's action. Free energy values obtained by well-tempered metadynamics simulations suggest that the neutral form is the only permeating protomer, consistent with experimental data. H-bond interactions of the drug with water molecules and membrane headgroups play a crucial role for permeation. The presence of the transmembrane potential, investigated here for the first time in a drug permeation study, does not qualitatively affect these conclusions.

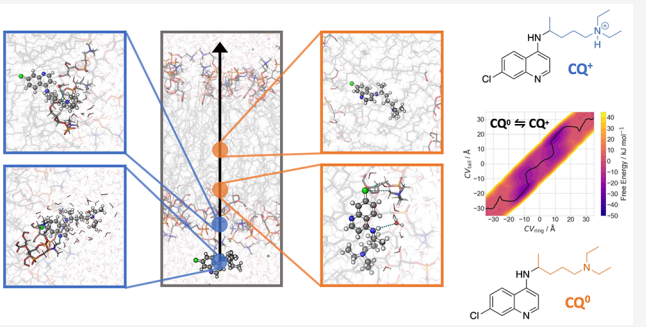

INTRODUCTION

The interaction of drugs with biological membranes impact dramatically on their mechanism of action. A typical example is the FDA-approved antimalarial drug chloroquine (**CQ**).[1,2] This drug also possesses antiviral,[3−5] antirheumatic,[6−8] and anti-inflammatory properties.[9,10] In fact, its beneficial effect stems from the drug's ability to reach the food vacuole, an acidic compartment of the parasite, so that the drug has to permeate several biological membranes.[11] The drug can feature three different protonation species at the extracellular pH (Chart 1), from the neutral one ($\mathbf{CQ^0}$), to the mono- ($\mathbf{CQ^+}$) and diprotonated ($\mathbf{CQ^{2+}}$) species (pK_{a1} and pK_{a2} are 8.1 and 10.4 at 310 K).[12]

CQ penetrates malaria-infected human erythrocytes by passive diffusion of the free base, which may become protonated and trapped inside the acidic vacuole with a pH value in the range of 4.5−4.9.[13,14] However, a detailed study of **CQ** binding to intact and lysed erythrocytes indicated that the mechanism of **CQ** accumulation in intact cells is actually a combination of ion trapping at acidic pH (a consequence of the basic nature of the drug and the pH gradient across the membrane) and binding to cell components.[15]

The analysis of **CQ** uptake into erythrocytes infected with drug-sensitive and resistant strains of the human malaria parasite *Plasmodium falciparum* revealed that uptake can be resolved into a nonsaturable and a saturable component.[16,17,75] Nonsaturable uptake in the submicromolar range[18] is non-specific and is attributed to low-affinity binding of **CQ** to plentiful cytosolic proteins.[19] Conversely, saturable uptake at nanomolar drug concentrations is important for antimalarial activity[18] and attributed to intracellular binding of **CQ** to ferriprotoporphyrin IX (FPIX), a product of parasite hemoglobin digestion.[16,20] FPIX is polymerized into an inert crystalline substance called hemozoin, but **CQ** inhibits this process causing a buildup of free FPIX and/or **CQ**−FPIX complex that will ultimately kill the parasite.[21−23] Thus, the intracellular uptake of **CQ** in malaria-infected cells is primarily due to passive diffusion followed by saturable binding of **CQ** to FPIX rather than active import by membrane transporters.[16,24]

The drugs' uptake requires about 1 h.[25,26,76] Permeation occurs by fast passive diffusion with a permeability coefficient of 7.2 cm s^{-1} for $\mathbf{CQ^0}$ at 310 K.[11,15,27] Only $\mathbf{CQ^0}$ permeates the membrane in spite of being extremely scarce in physiological conditions (about one part for 10,000).[15,27,77] While one can provide simple electrostatic arguments to explain this—charged molecules are not thermodynamically stable inside the hydrophobic part of the membrane—a molecular view of drug permeation, and in particular of the role of water for drug permeation, is still missing.

Received: August 25, 2023
Revised: October 11, 2023
Accepted: October 12, 2023
Published: November 10, 2023

Chart 1. Protomers of Chloroquine (CQ)[a]

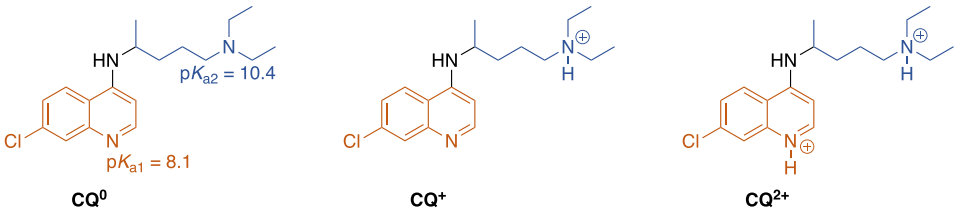

[a]The ring and tail moieties are colored in orange and blue, respectively.

For the past decade, a variety of state-of-the-art enhanced sampling methods have successfully described the structure, dynamics and energetics of small molecule permeation.[32−38] Here we use well-tempered metadynamics (WTMetaD), an exact method to calculate the free energies of a process as a function of appropriate collective variables,[39,40] to describe the process. Our calculations are carried out for the two species **CQ^0** and **CQ$^+$**, in model membranes with different compositions or in the presence of a transmembrane potential. **CQ^0** (and not **CQ$^+$**) passes the membrane, consistent with experimental evidence. The process is not qualitatively changed in the presence of the membrane potential.

METHODS

All calculations and most of the analyses were carried out with the GROMACS 2019.4 package interfaced with the PLUMED-2.5.3 plugin.[41−43]

Lipid Bilayer Preparation. A 2 × 37 pure POPC[78] bilayer (**M1**) and a 2 × 40 POPC/POPS[79] (**M2**) bilayer with 7:3 stoichiometry were generated using the CHARMM GUI web server[44] and inserted in a box of sizes 50 Å × 50 Å × 100 Å. A 30 Å thick water slabs were located on top of each leaflet. Eleven (35) Na^+ and 11 (11) Cl^- ions were added to **M1** (**M2**) so as to ensure electroneutrality and to keep the salt concentration of 150 mM, a value not too dissimilar from the extracellular fluid.[45] Overlapping water molecules were removed. **M1** and **M2** contained 23,423 and 24,752 atoms, respectively.

Molecular Dynamics Parameters. The AMBER Lipid 17,[46] TIP3P,[47] and Joung−Cheatham[48] force fields were used for the membranes, water molecules, and Na^+/Cl^- ions, respectively. As for the drugs, the GAFF2 force field was employed for bonded and van der Waals parameters of the drugs,[49] while the atomic partial charges were calculated using the RESP fit method at the HF/6-31G*//B3LYP/6-31G* level of theory.[50−52] Periodic boundary conditions were applied. Electrostatic interactions were calculated using the particle-mesh Ewald summation method with a real space cutoff of 10 Å.[53] Lennard-Jones interactions were truncated at the same cutoff value. An analytical correction for the potential energy and for the overall pressure taking into account the truncation of the Lennard-Jones interactions (implemented in GROMACS[41]) has been applied. All bonds involving hydrogen atoms were constrained using the LINCS algorithm.[54] An integration time step of 2 fs was used. The center of mass motion was removed separately for the lipids and aqueous phase every 100 steps. Unless differently stated, (i) constant temperature simulations were achieved by coupling the systems with a Nosé−Hoover thermostat, using a time constant of 0.5 ps;[55,56] (ii) constant pressure simulations were obtained using semi isotropic Parrinello−Rahman barostat at 1 bar, using a time constant of 1.0 ps and compressibility of 4.5 × 10^{-5} bar^{-1}.[57]

Molecular Dynamics Simulation of M1 and M2. The systems were first energy-minimized by 10,000 steepest descent steps. Then, they were heated up by 100 ps from 0 to 310 K by molecular dynamics with velocity rescale methods with a time constant of 0.1 ps.[58] Here, the lipid atoms were restrained to their position by harmonic restraints of 50 kJ mol^{-1} $Å^{-2}$. The systems were then unconstrained. Next, **M1** and **M2** underwent 60 and 110 ns *NPT* MD simulations, respectively. Some features of these simulations are reported in the Supporting Information.

Insertion of the Drugs. The drugs were placed into the aqueous phase at 35 Å along the membrane normal (*z*-axis in Figure 1) from the center of the membrane. We used the GROMACS insert-molecule module.[41] Also in this case, overlapping water molecules were removed. The resulting systems underwent 10 ns-long *NPT* simulations. The final configurations were used for subsequent calculations of the free energy. Selected configurations in which the ligand was located at around −40 Å from the center of the membrane along the *z*-axis ($z = 0$) were used for subsequent calculations of the diffusion coefficient. For the calculation of the diffusion coefficient, also a total of 1.275 μs *NVE* trajectories were collected (see Section S7 in the Supporting Information).

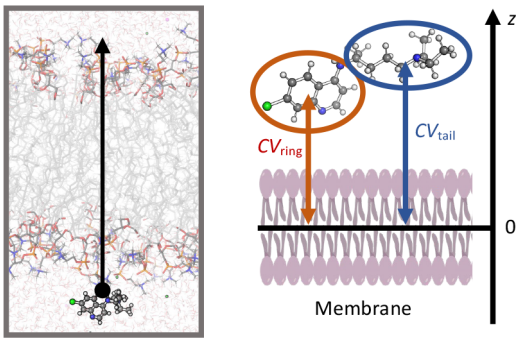

Figure 1. Permeation coordinate. Left: Snapshot of chloroquine in the presence of a lipid bilayer, schematically indicating the permeation coordinate with the black arrow. Right: The two collective variables, CV_{ring} and CV_{tail}, measure the distances of the ring/tail moieties of chloroquine with respect to the membrane center along the normal *z*-axis.

Free Energy Calculations. The free energy as a function of a specific collective variable was calculated by well-tempered metadynamics.[39] Our collective variables (CVs) are the distances between the drug's center of masses (COMs) and the COM of 40 selected membrane atoms, representing the center of the membrane. They correspond to the *z*-component of its direction vector (see Figure 1 which shows the *z*-axis).

https://doi.org/10.1021/acs.jcim.3c01363
J. Chem. Inf. Model. 2023, 63, 7124−7132

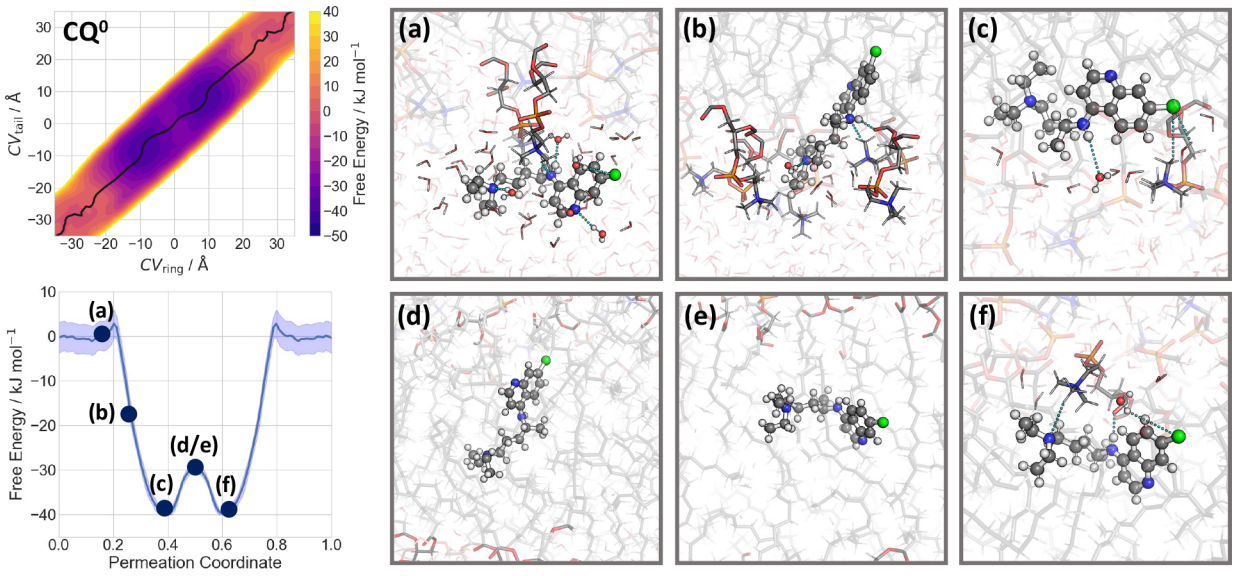

Figure 2. Permeation of CQ^0 through a POPC membrane. Left: the free energy of the process, calculated as a function of CV_{ring} and CV_{tail} (see Figure 1). The minimum free energy path is plotted as black line (top) and is shown in its one-dimensional representation below. (a–f) Representative snapshots of the CQ^0 permeation process across the POPC membrane. The associated free energies are indicated in the minimum free energy profile.

The center of the membrane is set to have $z = 0$. This CV has been used also in previous drug permeation studies:[32−38] Gaussians with 1.2 kJ mol^{-1} initial height and 0.5 Å sigma values were deposited every 2 ps, similarly to refs 36 and 59. The bias factor for CQ^+ (25) is larger than that for CQ^0 (20), because a higher free energy barrier of the charged species is expected. The bias potential was evaluated on a grid of spacing of 0.01 Å. The reweighting factor $c(t)$ was calculated on the fly. Free energy profiles were constructed through the reweighting scheme of ref 60.

Here, 4.5 μs were simulated for each system. The first 500 ns were not included in the analysis as in ref 60. Errors of the free energy profiles were estimated by block averaging with three blocks of the processed data (see Supporting Information). The free energy profiles were then symmetrized and checked for their asymmetry (see Supporting Information). The minimum free energy paths on the 2D free energy surface were determined by the string method.[61]

The calculations with the electric field were carried out using the GROMACS routine[41] to mimic the presence of a transmembrane potential. A potential of 10 mV $Å^{-1}$ was set. Not too dissimilar potentials have been used in other setups, such as the computational electrophysiology simulations.[62−65] Here, 3 μs were simulated with and without the electric field, using a simpler one-dimensional CV space (see Figure S14a in Supporting Information).

Calculated Properties. (i) The diffusion and the permeability coefficient were calculated as described in Section S7 of Supporting Information.[66,67] (ii) Radial distribution functions of the water-drug H-bonds were calculated from the well-tempered metadynamics runs for **M1**. All snapshots in which the drug was located in the aqueous phase with a distance larger than 30 Å from the membrane center (10,403 and 14,440 structures for CQ^0 and CQ^+, respectively) were used. (iii) The free energy differences between CQ^0 and CQ^+ were calculated as in refs 35 and 68. The free energy of CQ^0 is first shifted to account for its acid−base equilibrium in the aqueous phase, considering pK_{a2} (10.4) at the conditions of the simulation (neutral pH and temperature of 310 K).[80] The $CQ^0 \rightleftharpoons CQ^+$ free energy surface is then determined by weighting the individual free energy surfaces with respect to the calculated population of protomers as a function of CVs (see Supporting Information, Section S4 for details). (iv) The dipole moment of CQ^0 was calculated at the B3LYP/6-31G* level of theory using the Gaussian09 code.[69]

RESULTS AND DISCUSSION

As a first step, the free energy associated with the permeation of the **CQ** molecule is calculated using well-tempered metadynamics, which is an exact method to calculate the free energy landscapes as a function of apt CVs.[40] Previous studies have used either one or two CVs.[36,38,59] Choosing an additional CV has been shown to significantly improve the results.[36] Here, we choose the following CVs: the distances between the center of the membrane and the ring/tail moieties of **CQ** (Figure 1).

Permeation of CQ^0. MD simulations of CQ^0 (Chart 1) in explicit solvent and in the presence of the POPC membrane (Figures 1 and 2) show that all H-bond functional groups of CQ^0 interact with the solvent (Figure S3). After leaving the bulk solvent, the ring and tail moieties of CQ^0 interact with POPC headgroups, while the rest is still fully solvated (Figure 2a). Then, the ring moiety dives into the membrane (Figure 2b) and the tail interacts, in turn, with the POPC headgroups (Figure 2b). In this step, the free energy decreases by 20 kJ mol^{-1} (Figure 2, left). Subsequently, CQ^0 forms H-bonds with POPC headgroups and water molecules, while the remainder interacts with the hydrophobic core of the membrane (Figure 2c). This is the global free energy minimum (−40 kJ mol^{-1} lower than in the solvated state), located inside the membrane. Then, the free energy increases by 11 kJ mol^{-1}: CQ^0 is entirely inside the membrane, interacting exclusively with the hydrophobic core (Figures 2d and 2e). The second part of the translocation is, as expected, completely symmetrical with respect to the first part (Figure 2f). We conclude that CQ^0 is located at the water/membrane interfaces, so as to form H-

https://doi.org/10.1021/acs.jcim.3c01363
J. Chem. Inf. Model. 2023, 63, 7124−7132

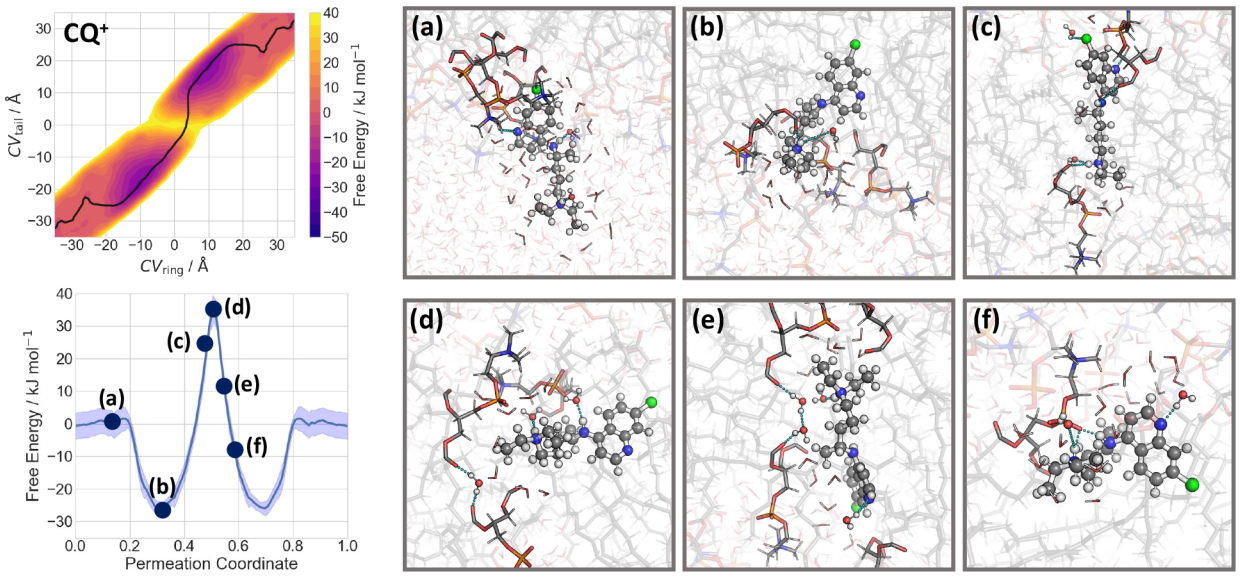

Figure 3. Permeation of CQ^+ through a POPC membrane. Left: the free energy of the process, calculated as a function of CV_{ring} and CV_{tail} (see Figure 1). The minimum free energy path is plotted as black line (top) and is shown in its one-dimensional representation below. (a–f) Representative snapshots of the CQ^+ permeation process across the POPC membrane. The associated free energies are indicated in the minimum free energy profile.

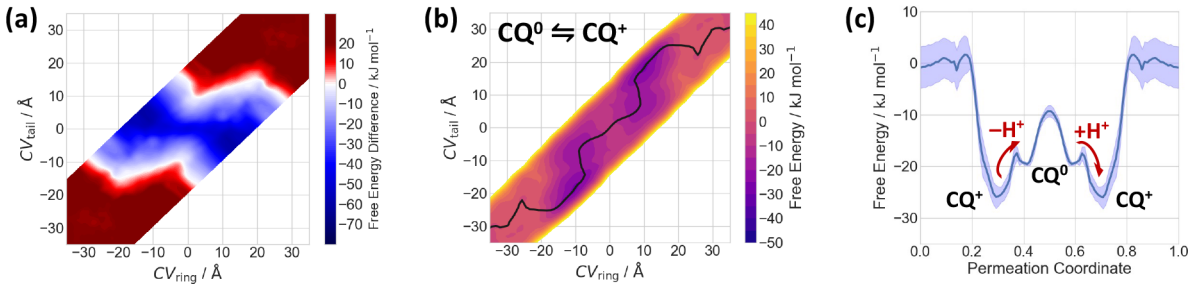

Figure 4. Protonation-dependent permeation of **CQ** through a POPC membrane. (a) The free energy difference of CQ^+ and CQ^0, as a function of CV_{ring} and CV_{tail} (see Figure 1). The calculated profile of CQ^0 is shifted with respect to the aqueous state, considering a solution pH of 7 and a pK_a value of 10.4 at 310 K. Red indicates a preferred protonated state (CQ^+), while blue indicates a preferred neutral state (CQ^0). (b) Free energy surface for the permeation of $CQ^0 \rightleftharpoons CQ^+$, as a function of the two CVs, weighted according to the calculated population of the corresponding protonation state. The minimum free energy path is shown as black line. (c) 1D minimum free energy path of the $CQ^0 \rightleftharpoons CQ^+$ free energy surface. Suggested positions for proton transfer are indicated as red arrows.

bond interactions with its polar moiety and hydrophobic with the rest. It can permeate from side to side in the submillisecond time scale, taking into account the barrier of about 10 kJ mol^{-1}. The experimental evidence also shows that the neutral molecule can permeate through the erythrocyte cell membrane. Thus, our results are consistent with these experiments, with the caveat that the latter were performed in a different environment than the one used here.

Protonated Species. The molecular mechanism of permeation of CQ^+ is similar to that of CQ^0. However, in this case the global minimum is far more solvated than in the case of the neutral molecule, most likely because the solvent stabilizes the charged molecule (Figure 3b). Here, the ring moiety interacts with the hydrophobic core of the membrane, while the charged tail of CQ^+ interacts with water molecules and POPC headgroups at the lipid/water interface. More importantly, the maximum free energy inside the membrane now shifts by as much as 35 kJ mol^{-1} with respect to the solvent state. This is caused by the destabilization of the charged molecule within the membrane along with membrane deformation and water defects (Figure 3c–f). The total energy barrier for membrane translocation is 60 kJ mol^{-1}. Thus, we conclude that, consistent with experiment, the protonated CQ^+ does not cross the membrane, within the limitations that different membranes have been used.

The calculated free energy difference between CQ^0 and CQ^+ suggests that the protonated species is not stable within the membrane (Figure 4a). The reversal point is located at the lipid/water interface, when the charged tail of CQ^+ enters the hydrophobic core of the membrane ($CV_{tail} \approx \pm 10$ Å). The permeation mechanism can be described as follows: the protonated CQ^+ dives into the membrane with its ring moiety, while the tail moiety is still sufficiently solvated at the lipid/water interface (Figures 3b and 4). As discussed above, this corresponds to the global minimum of CQ^+. When the tail moiety enters the hydrophobic core of the membrane, the proton is expected to be transferred to the solution phase. Both water molecules and POPC headgroups interact with the tail moiety and could act as proton acceptors (Figure 3b). The neutral CQ^0 is then located inside the membrane (Figure 2c) and is able to pass the membrane center. The total barrier for membrane translocation is 16 kJ mol^{-1}, consistent with the

https://doi.org/10.1021/acs.jcim.3c01363
J. Chem. Inf. Model. 2023, 63, 7124−7132

experimental evidence that CQ^0 can pass the membrane. Upon leaving the membrane, the amine nitrogen gets reprotonated so that the tail moiety exits the hydrophobic core of the membrane first, followed by the ring moiety to complete the permeation process.

In a recent study, the permeation process of a weak base, propranolol, was investigated by MD simulations at constant pH, allowing for dynamic protonation of the molecule in the inhomogeneous environments.[70] Similar to our findings, the change in protonation state was observed at the lipid/water interface and the free energy profile proceeds along the energetically favorable protomer in the different phases.[70] We conclude that the protonation states of **CQ** (or similar drug-like molecules) can have a significant impact on the permeation mechanism and energetics even if only the neutral molecule is able to cross the membrane center.

Impact of Membrane Composition on Permeation. Next, the permeation process of CQ^0 was investigated across a POPC/POPS mixed bilayer. We used a deliberately high concentration of POPS (30%) in order to study the effect of negatively charged membranes. However, we do not propose this as an universal model of cell membranes, which present great variability in their composition.

The mechanism of permeation across the POPC/POPS mixed bilayer is similar to that of the pure POPC membrane. However, quantitatively, the energetics of the permeation process differs slightly in the headgroup regions (Figure 5).

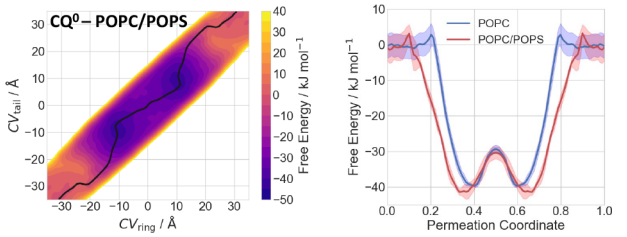

Figure 5. Effect of the membrane composition on the permeation of CQ^0. Left: Free energy surface for the permeation of CQ^0 through a POPC/POPS membrane, as a function of the CV_{ring} and CV_{tail}. The minimum free energy path is shown as black line. Right: 1D minimum free energy path of the free energy surface for CQ^0 permeating POPC (blue) and mixed POPC/POPS (red).

After leaving the bulk solvent, both the ring and tail moieties of CQ^0 interact with the POPC/POPS headgroups, while the remaining part of the molecule is still fully solvated (Figures S12a and S13a). The free energy increases slightly by 7 kJ mol^{-1}. The increase in free energy is more pronounced than for the pure POPC membrane, possibly due to the disruption of the rather strong interactions between the POPS headgroups (which are negatively charged) and water molecules. Then, the ring moiety dives into the membrane and the other moiety interacts, in turn, with POPC/POPS headgroups (Figures S12b and S13b). The free energy decreases by 20 kJ mol^{-1}. Next, the drug is inside the membrane: the molecule forms H-bonds with POPC/POPS headgroups and water molecules, while the rest interacts with the hydrophobic core of the membrane (Figures S12c and S13c). This is the global free energy minimum (−42 kJ mol^{-1} lower than in the solvated state). Then, the free energy increases by 12 kJ mol^{-1} when the molecule is completely inside the membrane, interacting only with the hydrophobic core (Figures S12d and S13d). The second part of the translocation is, as expected, symmetrical with respect to the first part. Thus, our simulations suggest that the drug is located at the water/membrane interfaces, so as to form H-bond interactions with its polar moiety and hydrophobic with the rest.

Impact of External Potential on Permeation. The effect of the membrane potential on permeation has not been investigated so far, to the best of our knowledge. Here, we compare the energetics of the permeation of CQ^0 with and without an external electric field (E) of 10 mV $Å^{-1}$ along the POPC membrane. Our field value is not too dissimilar to that widely used in computational electrophysiology setups.[62−65] To a first approximation, we expect changes in the potential energy of the process of the order of the $2E{\cdot}\mu$ ($\approx$ 2−3 kJ mol^{-1}), where μ = 5.8 D is used for the dipole moment of CQ^0. Therefore, even fields much larger than the physiological ones ($\approx$0.5−3 mV $Å^{-1}$)[45] are unlikely to drastically affect permeation. The free energy calculations of CQ^0 permeation using CV_{CQ}[81] show that this is indeed the case (Figure 6). The

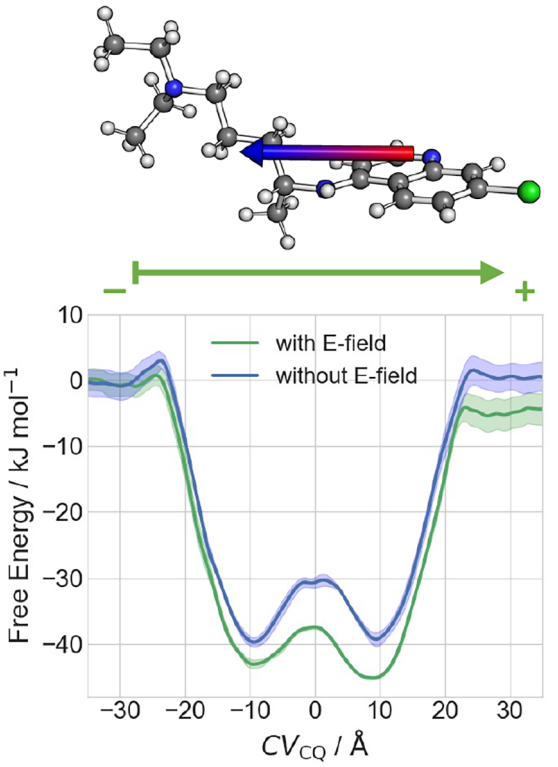

Figure 6. Effect of the external potential on permeation. Top: Ball-and-stick representation of CQ^0 showing its dipole moment as an arrow from negative (red) to positive (blue) charge distribution. Bottom: Comparison of free energies with and without an external field for CQ^0 permeation through the POPC membrane. The direction of the external field is shown as an arrow.

first free energy minimum is −43 kJ mol^{-1} lower than the value in the solvated state, and 3 kJ mol^{-1} lower than the value without the external electric field. Thus, CQ^0 slightly prefers the lipid phase when an E-field is taken into account. The free energy increases by 7 kJ mol^{-1} when the molecule is completely inside the membrane. The second free energy minimum is even lower (−46 kJ mol^{-1}). This asymmetry arises from the preferred orientation of CQ^0 along the direction of E (Figure S14). We conclude that the effect of the external electric field is of minor importance for CQ^0 permeation under

https://doi.org/10.1021/acs.jcim.3c01363
J. Chem. Inf. Model. 2023, 63, 7124−7132

physiological conditions. As a perspective of our work, one could extend the investigations in the presence of the external membrane potential to a comprehensive set of ionizable drugs (such as those reported in ref 71). These would lead to a more robust conclusion.

Permeability Coefficients. As a final step, we calculated the permeability coefficient from the inhomogeneous solubility-diffusion model. The position-dependent diffusion coefficients are given in the Supporting Information. The permeability coefficients of $\mathbf{CQ^0}$ are 38.2 ± 7.8 cm s^{-1} and 44 ± 12 cm s^{-1} for the permeation through the POPC and the POPC/POPS model membranes, respectively. Considering the protonation-dependent permeation process ($\mathbf{CQ^0} \rightleftharpoons \mathbf{CQ^+}$), the permeability coefficient amounts to 26.0 ± 6.0 cm s^{-1}. The use of more than one CVs for a proper description of the permeation path free energy (and thus the permeability coefficient) might be crucial for conformationally flexible drugs. In this study, two CVs were required for $\mathbf{CQ^+}$, possibly because the charged tail and ring moieties prefer an aqueous and a hydrophobic environment, respectively (see Figure 3). Instead, in $\mathbf{CQ^0}$, where the tail is neutral, one CV was sufficient (see Table S2 in the Supporting Information). The difference between the experimental value (7.2 cm s^{-1} at 310 K for the human erythrocyte membrane)[11,15] can be ascribed, at least in part, to the different chemical environments: the real cell membrane differs from our model membranes in several aspects. Most importantly, it features a high content of cholesterol that can significantly affect membrane permeability, usually lowering its value.[72,73] In addition, our models also lack sphingolipids that are charged groups and that usually increase the permeability.[74] So, in the end the membrane permeability will be modified by these chemicals in a highly nontrivial manner.

CONCLUSIONS

In conclusion, we present a study of chloroquine permeability along permeation through model membranes. The calculated permeability of the drug is about three to six times higher than experimentally found in biological membranes. Previous drug permeation studies predicted permeabilities with errors similar to that found here.[32,33,36,38] The difference might be ascribed, at least in part, by the highly diverse environments and by possible changes due to dynamic protonation of the drug, here not included.[70] In addition, we show that both the neutral ($\mathbf{CQ^0}$) and the protonated ($\mathbf{CQ^+}$) species are partially solvated in their global free energy minima at the membrane/water interface. However, while $\mathbf{CQ^0}$ can cross the hydrophobic core of the membrane in the absence of any H-bond interactions, $\mathbf{CQ^+}$ requires these interactions at its charged moiety in the permeation process. Consequently, $\mathbf{CQ^0}$ is the only species able to cross the membrane in a time scale compatible with experiments. The impact of cell membrane potential is negligible.

ASSOCIATED CONTENT

Data Availability Statement

The free energy calculations were carried out with the GROMACS 2019.4 package (https://www.gromacs.org/) interfaced with the PLUMED-2.5.3 plugin (https://www.plumed.org/). Parameter and topology files, starting configurations, and input files for the free energy calculations are provided in the Supporting Information.

Supporting Information

The Supporting Information is available free of charge at https://pubs.acs.org/doi/10.1021/acs.jcim.3c01363.

Some features of the classical MD simulations of the membrane models **M1** and **M2**; hydrogen bond analysis of **CQ** in the aqueous phase; detailed analysis of free energy surfaces; representative snapshots showing the permeation across the membrane models; description of the calculation of the $\mathbf{CQ^0} \rightleftharpoons \mathbf{CQ^+}$ free energy surface; computational details on the calculation of the diffusion coefficients and permeability coefficients (PDF)

Parameter and topology files, starting configurations, and input files for the free energy calculations (ZIP)

AUTHOR INFORMATION

Corresponding Author

Paolo Carloni − *Computational Biomedicine, Institute of Advanced Simulations IAS-5/Institute for Neuroscience and Medicine INM-9, Forschungszentrum Jülich GmbH, 52428 Jülich, Germany; Department of Physics, RWTH Aachen University, Aachen 52062, Germany;* orcid.org/0000-0002-9010-0149; Email: p.carloni@fz-juelich.de

Authors

Mirko Paulikat − *Computational Biomedicine, Institute of Advanced Simulations IAS-5/Institute for Neuroscience and Medicine INM-9, Forschungszentrum Jülich GmbH, 52428 Jülich, Germany;* orcid.org/0000-0001-8403-2138

GiovanniMaria Piccini − *Institute of Technical and Macromolecular Chemistry, RWTH Aachen University, 52074 Aachen, Germany*

Emiliano Ippoliti − *Computational Biomedicine, Institute of Advanced Simulations IAS-5/Institute for Neuroscience and Medicine INM-9, Forschungszentrum Jülich GmbH, 52428 Jülich, Germany;* orcid.org/0000-0001-5513-8056

Giulia Rossetti − *Computational Biomedicine, Institute of Advanced Simulations IAS-5/Institute for Neuroscience and Medicine INM-9 and Jülich Supercomputing Centre (JSC), Forschungszentrum Jülich GmbH, 52428 Jülich, Germany; Department of Neurology, RWTH Aachen University, Aachen 52062, Germany;* orcid.org/0000-0002-2032-4630

Fabio Arnesano − *Department of Chemistry, University of Bari "Aldo Moro", Bari 70125, Italy;* orcid.org/0000-0002-8399-0964

Complete contact information is available at: https://pubs.acs.org/10.1021/acs.jcim.3c01363

Notes

The authors declare no competing financial interest.

ACKNOWLEDGMENTS

The authors gratefully acknowledge the Gauss Centre for Supercomputing e.V. (www.gauss-centre.eu) and the Jülich Supercomputer Center for providing the computing time for this project. We also thank the University of Bari and the Italian Ministero dell'Università e della Ricerca (PRIN 2017WBZFHL to F.A.) for support. G.R. and P.C. acknowledge the Helmholtz European Partnering fundings for the project "Innovative high-performance computing approaches for molecular neuromedicine:, as well as the Joint Lab "Supercomputing and Modeling for the Human Brain" of the

Helmholtz Association, Germany. G.R. also acknowledges the Federal Ministry of Education and Research (BMBF) and the state of North Rhine-Westphalia as part of the NHR Program. Open access publication fee funded by the Deutsche Forschungsgemeinschaft (DFG, German Research Foundation), No. 491111487.

REFERENCES

(1) Homewood, C. A.; Warhurst, D. C.; Peters, W.; Baggaley, V. C. Lysosomes, pH and the Anti-malarial Action of Chloroquine. *Nature* **1972**, *235*, 50−52.
(2) Krogstad, D. J.; Schlesinger, P. H. A perspective on antimalarial action: Effects of weak bases on Plasmodium falciparum. *Biochem. Pharmacol.* **1986**, *35*, 547−552.
(3) Savarino, A.; Boelaert, J. R.; Cassone, A.; Majori, G.; Cauda, R. Effects of chloroquine on viral infections: an old drug against today's diseases. *Lancet Infect. Dis.* **2003**, *3*, 722−727.
(4) Keyaerts, E.; Li, S.; Vijgen, L.; Rysman, E.; Verbeeck, J.; Van Ranst, M. V.; Maes, P. Antiviral Activity of Chloroquine against Human Coronavirus OC43 Infection in Newborn Mice. *Antimicrob. Agents Chemother.* **2009**, *53*, 3416−3421.
(5) Farias, K. J. S.; Machado, P. R. L.; Muniz, J. A. P. C.; Imbeloni, A. A.; da Fonseca, B. A. L. Antiviral Activity of Chloroquine Against Dengue Virus Type 2 Replication in *Aotus* Monkeys. *Viral Immunol.* **2015**, *28*, 161−169.
(6) Salmeron, G.; Lipsky, P. Immunosuppressive potential of antimalarials. *Am. J. Med.* **1983**, *75*, 19−24.
(7) Rynes, R. I. Antimalarial drugs in the treatment of rheumatological diseases. *Rheumatology* **1997**, *36*, 799−805.
(8) Rainsford, K. D.; Parke, A. L.; Clifford-Rashotte, M.; Kean, W. F. Therapy and pharmacological properties of hydroxychloroquine and chloroquine in treatment of systemic lupus erythematosus, rheumatoid arthritis and related diseases. *Inflammopharmacology* **2015**, *23*, 231−269.
(9) Karres, I.; Kremer, J.-P.; Dietl, I.; Steckholzer, U.; Jochum, M.; Ertel, W. Chloroquine inhibits proinflammatory cytokine release into human whole blood. *Am. J. Physiol. Regul. Integr. Comp. Physiol.* **1998**, *274*, R1058−R1064.
(10) Park, J.; Kwon, D.; Choi, C.; Oh, J.-W.; Benveniste, E. N. Chloroquine induces activation of nuclear factor-B and subsequent expression of pro-inflammatory cytokines by human astroglial cells. *J. Neurochem.* **2003**, *84*, 1266−1274.
(11) Macintyre, A. C.; Cutler, D. J. Kinetics of Chloroquine Uptake into Isolated Rat Hepatocytes. *J. Pharm. Sci.* **1993**, *82*, 592−600.
(12) Warhurst, D. C.; Steele, J. C.; Adagu, I. S.; Craig, J. C.; Cullander, C. Hydroxychloroquine is much less active than chloroquine against chloroquine-resistant *Plasmodium falciparum*, in agreement with its physicochemical properties. *J. Antimicrob. Chemother.* **2003**, *52*, 188−193.
(13) Ginsburg, H.; Stein, W. Kinetic modelling of chloroquine uptake by malaria-infected erythrocytes. *Biochem. Pharmacol.* **1991**, *41*, 1463−1470.
(14) Hayward, R.; Saliba, K. J.; Kirk, K. The pH of the digestive vacuole of *Plasmodium falciparum* is not associated with chloroquine resistance. *J. Cell Sci.* **2006**, *119*, 1016−1025.
(15) Ferrari, V.; Cutler, D. J. Uptake of chloroquine by human erythrocytes. *Biochem. Pharmacol.* **1990**, *39*, 753−762.
(16) Bray, P. G.; Mungthin, M.; Ridley, R. G.; Ward, S. A. Access to Hematin: The Basis of Chloroquine Resistance. *Mol. Pharmacol.* **1998**, *54*, 170−179.
(17) Ginsburg, H.; Ward, S.; Bray, P. An Integrated Model of Chloroquine Action. *Parasitol. Today* **1999**, *15*, 357−360.
(18) Fitch, C. D. *Plasmodium falciparum* in Owl Monkeys: Drug Resistance and Chloroquine Binding Capacity. *Science* **1970**, *169*, 289−290.
(19) Dorn, A.; Vippagunta, S. R.; Matile, H.; Bubendorf, A.; Vennerstrom, J. L.; Ridley, R. G. A Comparison and Analysis of Several Ways to Promote Haematin (Haem) Polymerisation and an Assessment of Its Initiation In Vitro. *Biochem. Pharmacol.* **1998**, *55*, 737−747.
(20) Chou, A. C.; Chevli, R.; Fitch, C. D. Ferriprotoporphyrin IX Fulfills the Criteria for Identification as the Chloroquine Receptor of Malaria Parasites. *Biochemistry* **1980**, *19*, 1543−1549.
(21) Dorn, A.; Stoffel, R.; Matile, H.; Bubendorf, A.; Ridley, R. G. Malarial haemozoin/-haematin supports haem polymerization in the absence of protein. *Nature* **1995**, *374*, 269−271.
(22) Sullivan, D. J.; Gluzman, I. Y.; Russell, D. G.; Goldberg, D. E. On the molecular mechanism of chloroquine's antimalarial action. *Proc. Natl. Acad. Sci. U. S. A.* **1996**, *93*, 11865−11870.
(23) Weissbuch, I.; Leiserowitz, L. Interplay Between Malaria, Crystalline Hemozoin Formation, and Antimalarial Drug Action and Design. *Chem. Rev.* **2008**, *108*, 4899−4914.
(24) Bray, P. G.; Janneh, O.; Raynes, K. J.; Mungthin, M.; Ginsburg, H.; Ward, S. A. Cellular Uptake of Chloroquine Is Dependent on Binding to Ferriprotoporphyrin IX and Is Independent of NHE Activity in Plasmodium falciparum. *J. Cell Biol.* **1999**, *145*, 363−376.
(25) Geary, T. G.; Jensen, J. B.; Ginsburg, H. Uptake of [3H]chloroquine by drug-sensitive and -resistant strains of the human malaria parasite Plasmodium falciparum. *Biochem. Pharmacol.* **1986**, *35*, 3805−3812.
(26) Reiling, S. J.; Rohrbach, P. Uptake of a fluorescently tagged chloroquine analogue is reduced in CQ-resistant compared to CQ-sensitive Plasmodium falciparum parasites. *Malar. J.* **2019**, *18*, 342.
(27) Ferrari, V.; Cutler, D. J. Kinetics and thermodynamics of chloroquine and hydroxychloroquine transport across the human erythrocyte membrane. *Biochem. Pharmacol.* **1991**, *41*, 23−30.
(28) Petelska, A. D.; Figaszewski, Z. A. Effect of pH on the Interfacial Tension of Lipid Bilayer Membrane. *Biophys. J.* **2000**, *78*, 812−817.
(29) Petelska, A. D.; Figaszewski, Z. A. Effect of pH on the interfacial tension of bilayer lipid membrane formed from phosphatidylcholine or phosphatidylserine. *Biochim. Biophys. Acta Biomembr.* **2002**, *1561*, 135−146.
(30) Zhou, Y.; Raphael, R. M. Solution pH Alters Mechanical and Electrical Properties of Phosphatidylcholine Membranes: Relation between Interfacial Electrostatics, Intramembrane Potential, and Bending Elasticity. *Biophys. J.* **2007**, *92*, 2451−2462.
(31) Deplazes, E.; Poger, D.; Cornell, B.; Cranfield, C. G. The effect of hydronium ions on the structure of phospholipid membranes. *Phys. Chem. Chem. Phys.* **2018**, *20*, 357−366.
(32) Lee, C. T.; Comer, J.; Herndon, C.; Leung, N.; Pavlova, A.; Swift, R. V.; Tung, C.; Rowley, C. N.; Amaro, R. E.; Chipot, C.; Wang, Y.; Gumbart, J. C. Simulation-Based Approaches for Determining Membrane Permeability of Small Compounds. *J. Chem. Inf. Model.* **2016**, *56*, 721−733.
(33) Dickson, C. J.; Hornak, V.; Pearlstein, R. A.; Duca, J. S. Structure-kinetic relationships of passive membrane permeation from multiscale modeling. *J. Am. Chem. Soc.* **2017**, *139*, 442−452.
(34) Bennion, B. J.; Be, N. A.; McNerney, M. W.; Lao, V.; Carlson, E. M.; Valdez, C. A.; Malfatti, M. A.; Enright, H. A.; Nguyen, T. H.; Lightstone, F. C.; Carpenter, T. S. Predicting a Drug's Membrane Permeability: A Computational Model Validated with in Vitro Permeability Assay Data. *J. Phys. Chem. B* **2017**, *121*, 5228−5237.
(35) DeMarco, K. R.; Bekker, S.; Clancy, C. E.; Noskov, S. Y.; Vorobyov, I. Digging into lipid membrane permeation for cardiac ion channel blocker d-sotalol with all-atom simulations. *Front. Pharmacol.* **2018**, *9*, 00026.
(36) Sun, R.; Han, Y.; Swanson, J. M.; Tan, J. S.; Rose, J. P.; Voth, G. A. Molecular transport through membranes: Accurate permeability coefficients from multidimensional potentials of mean force and local diffusion constants. *J. Chem. Phys.* **2018**, *149*, 072310.
(37) Martinotti, C.; Ruiz-Perez, L.; Deplazes, E.; Mancera, R. L. Molecular Dynamics Simulation of Small Molecules Interacting with Biological Membranes. *ChemPhysChem* **2020**, *21*, 1486−1514.
(38) Shoji, A.; Kang, C.; Fujioka, K.; Rose, J. P.; Sun, R. Assessing the Intestinal Permeability of Small Molecule Drugs via Diffusion

https://doi.org/10.1021/acs.jcim.3c01363
J. Chem. Inf. Model. 2023, 63, 7124−7132

Motion on a Multidimensional Free Energy Surface. *J. Chem. Theory Comput.* **2022**, *18*, 503−515.
(39) Barducci, A.; Bussi, G.; Parrinello, M. Well-Tempered Metadynamics: A Smoothly Converging and Tunable Free-Energy Method. *Phys. Rev. Lett.* **2008**, *100*, No. 020603.
(40) Dama, J. F.; Parrinello, M.; Voth, G. A. Well-tempered metadynamics converges asymptotically. *Phys. Rev. Lett.* **2014**, *112*, 240602.
(41) Abraham, M. J.; Murtola, T.; Schulz, R.; Páll, S.; Smith, J. C.; Hess, B.; Lindahl, E. GROMACS: High performance molecular simulations through multi-level parallelism from laptops to supercomputers. *SoftwareX* **2015**, *1−2*, 19−25.
(42) Tribello, G. A.; Bonomi, M.; Branduardi, D.; Camilloni, C.; Bussi, G. PLUMED 2: New feathers for an old bird. *Comput. Phys. Commun.* **2014**, *185*, 604−613.
(43) The PLUMED consortium. Promoting transparency and reproducibility in enhanced molecular simulations. *Nat. Methods* **2019**, *16*, 670−673.
(44) Wu, E. L.; Cheng, X.; Jo, S.; Rui, H.; Song, K. C.; Dávila-Contreras, E. M.; Qi, Y.; Lee, J.; Monje-Galvan, V.; Venable, R. M.; Klauda, J. B.; Im, W. CHARMM-GUI *Membrane Builder* toward realistic biological membrane simulations. *J. Comput. Chem.* **2014**, *35*, 1997−2004.
(45) Alberts, B.; Johnson, A.; Lewis, J.; Morgan, D.; Raff, M.; Roberts, K.; Walter, P. In *Molecular Biology of the Cell*, 6th ed.; Wilson, J., Hunt, T., Eds.; W.W. Norton & Company: 2017; DOI: 10.1201/9781315735368
(46) Dickson, C. J.; Madej, B. D.; Skjevik, Å. A.; Betz, R. M.; Teigen, K.; Gould, I. R.; Walker, R. C. Lipid14: The amber lipid force field. *J. Chem. Theory Comput.* **2014**, *10*, 865−879.
(47) Jorgensen, W. L.; Chandrasekhar, J.; Madura, J. D.; Impey, R. W.; Klein, M. L. Comparison of simple potential functions for simulating liquid water. *J. Chem. Phys.* **1983**, *79*, 926−935.
(48) Joung, I. S.; Cheatham, T. E. Determination of Alkali and Halide Monovalent Ion Parameters for Use in Explicitly Solvated Biomolecular Simulations. *J. Phys. Chem. B* **2008**, *112*, 9020−9041.
(49) Wang, J.; Wolf, R. M.; Caldwell, J. W.; Kollman, P. A.; Case, D. A. Development and testing of a general amber force field. *J. Comput. Chem.* **2004**, *25*, 1157−1174.
(50) Bayly, C. I.; Cieplak, P.; Cornell, W.; Kollman, P. A. A well-behaved electrostatic potential based method using charge restraints for deriving atomic charges: the RESP model. *J. Phys. Chem.* **1993**, *97*, 10269−10280.
(51) Becke, A. D. Density-functional thermochemistry. III. The role of exact exchange. *J. Chem. Phys.* **1993**, *98*, 5648−5652.
(52) Stephens, P. J.; Devlin, F. J.; Chabalowski, C. F.; Frisch, M. J. Ab Initio Calculation of Vibrational Absorption and Circular Dichroism Spectra Using Density Functional Force Fields. *J. Phys. Chem.* **1994**, *98*, 11623−11627.
(53) Darden, T.; York, D.; Pedersen, L. Particle mesh Ewald: An $N \cdot log\ (N)$method for Ewald sums in large systems. *J. Chem. Phys.* **1993**, *98*, 10089−10092.
(54) Hess, B.; Bekker, H.; Berendsen, H. J. C.; Fraaije, J. G. E. M. LINCS: A linear constraint solver for molecular simulations. *J. Comput. Chem.* **1997**, *18*, 1463−1472.
(55) Nosé, S. A unified formulation of the constant temperature molecular dynamics methods. *J. Chem. Phys.* **1984**, *81*, 511−519.
(56) Hoover, W. G. Canonical dynamics: Equilibrium phase-space distributions. *Phys. Rev. A* **1985**, *31*, 1695−1697.
(57) Parrinello, M.; Rahman, A. Polymorphic transitions in single crystals: A new molecular dynamics method. *J. Appl. Phys.* **1981**, *52*, 7182−7190.
(58) Bussi, G.; Donadio, D.; Parrinello, M. Canonical sampling through velocity rescaling. *J. Chem. Phys.* **2007**, *126*, No. 014101.
(59) Ghaemi, Z.; Alberga, D.; Carloni, P.; Laio, A.; Lattanzi, G. Permeability Coefficients of Lipophilic Compounds Estimated by Computer Simulations. *J. Chem. Theory Comput.* **2016**, *12*, 4093−4099.
(60) Tiwary, P.; Parrinello, M. A time-independent free energy estimator for metadynamics. *J. Phys. Chem. B* **2015**, *119*, 736−742.
(61) E, W.; Ren, W.; Vanden-Eijnden, E. Simplified and improved string method for computing the minimum energy paths in barrier-crossing events. *J. Chem. Phys.* **2007**, *126*, 164103.
(62) Kutzner, C.; Grubmüller, H.; de Groot, B. L.; Zachariae, U. Computational Electrophysiology: The Molecular Dynamics of Ion Channel Permeation and Selectivity in Atomistic Detail. *Biophys. J.* **2011**, *101*, 809−817.
(63) Kutzner, C.; Köpfer, D. A.; Machtens, J.-P.; de Groot, B. L.; Song, C.; Zachariae, U. Insights into the function of ion channels by computational electrophysiology simulations. *Biochim. Biophys. Acta* **2016**, *1858*, 1741−1752.
(64) Kopec, W.; Köpfer, D. A.; Vickery, O. N.; Bondarenko, A. S.; Jansen, T. L. C.; de Groot, B. L.; Zachariae, U. Direct knock-on of desolvated ions governs strict ion selectivity in K^+ channels. *Nat. Chem.* **2018**, *10*, 813−820.
(65) Schackert, F. K.; Biedermann, J.; Abdolvand, S.; Minniberger, S.; Song, C.; Plested, A. J. R.; Carloni, P.; Sun, H. Mechanism of Calcium Permeation in a Glutamate Receptor Ion Channel. *J. Chem. Inf. Model.* **2023**, *63*, 1293−1300.
(66) Gaalswyk, K.; Awoonor-Williams, E.; Rowley, C. N. Generalized Langevin Methods for Calculating Transmembrane Diffusivity. *J. Chem. Theory Comput.* **2016**, *12*, 5609−5619.
(67) Venable, R. M.; Krämer, A.; Pastor, R. W. Molecular Dynamics Simulations of Membrane Permeability. *Chem. Rev.* **2019**, *119*, 5954−5997.
(68) MacCallum, J. L.; Bennett, W. F. D.; Tieleman, D. P. Distribution of Amino Acids in a Lipid Bilayer from Computer Simulations. *Biophys. J.* **2008**, *94*, 3393−3404.
(69) Frisch, M. J. et al.. *Gaussian 09, Revision A.02.*; Gaussian, Inc.: Wallington, CT, 2009.
(70) Yue, Z.; Li, C.; Voth, G. A.; Swanson, J. M. J. Dynamic Protonation Dramatically Affects the Membrane Permeability of Drug-like Molecules. *J. Am. Chem. Soc.* **2019**, *141*, 13421−13433.
(71) Hermann, K. F.; Neuhaus, C. S.; Micallef, V.; Wagner, B.; Hatibovic, M.; Aschmann, H. E.; Paech, F.; Alvarez-Sanchez, R.; Krämer, S. D.; Belli, S. Kinetics of lipid bilayer permeation of a series of ionisable drugs and their correlation with human transporter-independent intestinal permeability. *Eur. J. Pharm. Sci.* **2017**, *104*, 150−161.
(72) Zhang, X.; Barraza, K. M.; Beauchamp, J. L. Cholesterol provides nonsacrificial protection of membrane lipids from chemical damage at air−water interface. *Proc. Natl. Acad. Sci. U. S. A.* **2018**, *115*, 3255−3260.
(73) Blosser, M. C.; So, J.; Madani, M. S.; Malmstadt, N. Effect of Cholesterol on Permeability of Carbon Dioxide across Lipid Membranes. *bioRxiv* 2020.
(74) Jiménez-Rojo, N.; Sot, J.; Viguera, A.; Collado, M. I.; Torrecillas, A.; Gómez-Fernández, J.; Goñi, F.; Alonso, A. Membrane Permeabilization Induced by Sphingosine: Effect of Negatively Charged Lipids. *Biophys. J.* **2014**, *106*, 2577−2584.
(75) The uptake is different for healthy erythrocytes. Indeed, the saturable high-affinity component of **CQ** (i.e., FPIX) is absent or deficient in uninfected cells due to lack of hemoglobin degradation by the parasite.[18] As a matter of fact, there is no evidence of saturation of **CQ** transport in uninfected erythrocytes.[15]
(76) Using tritiated or fluorescently tagged **CQ**, at least two phases were observed: an extremely rapid short phase (<30 s), followed by a slower phase leading to steady state within 1 h.[25,26]
(77) Although the concentration of individual drug species cannot be directly measured, fitting drug uptake data allowed to separate the permeability coefficient of $\mathbf{CQ^0}$ from that of $\mathbf{CQ^+}$, as described in ref15. The experiments for the determination of the permeability coefficients were conducted in a narrow pH range (from 7.2 to 7.8). Thus, the pH was not significantly changed. This is an important point since changing the pH can alter the properties of the lipid bilayer, as already pointed out in the literature.[28−31]
(78) 1-Palmitoyl-2-oleoyl-*sn*-glycero-3-phosphocholine.

(79) 1-Palmitoyl-2-oleoyl-*sn*-glycero-3-phosphoserine.
(80) We assume that the doubly charged $\mathbf{CQ}^{2+}$ is not stable in the membrane, so that $\mathbf{CQ}^{2+}$ is expected to be deprotonated in the aqueous phase to form the $\mathbf{CQ}^{+}$ before entering the membrane. Under this assumption, the free energy surface would only be slightly shifted without an impact on the permeation mechanism.
(81) In these simulations, we used a simplified one-dimensional CV space, representing the distance of the center of mass of the entire $\mathbf{CQ}^{0}$ molecule to the center of the membrane (see Figure S14a in Supporting Information).

https://doi.org/10.1021/acs.jcim.3c01363
J. Chem. Inf. Model. 2023, 63, 7124−7132